atmosphere

Article

Mesoscale Characteristics of Exceptionally Heavy Rainfall during 4–6 May 2023 in Jiangxi, China

An Xiao [1,2], Jiusheng Shan [1,2,*], Hong Chen [3], Huimeng Bao [1,2], Houjie Xia [1,2], Zhehua Li [4] and Xianyao Liu [1,2]

[1] Weather Forecast Open Laboratory of Jiangxi Meteorological Bureau, Nanchang 330096, China; mrxiaoan@sohu.com (A.X.); baohuimeng@126.com (H.B.); xiahoulove@126.com (H.X.); flashlxy@foxmail.com (X.L.)
[2] Jiangxi Meteorological Observatory, Nanchang 330096, China
[3] Tianjin Meteorological Observatory, Tianjin 210074, China; chenhongfengye@163.com
[4] Shangrao Meteorological Burean, Shangrao 334000, China; lzhehua@163.com
* Correspondence: sjs861002@163.com

Abstract: A long-lasting rainfall event exceeding historical extremes took place in Jiangxi, China, from May 4 to 6, 2023. Because of the concentrated duration of precipitation, it led to significant water accumulation in the northern, central, and southern regions of Jiangxi. The objective of this study was to investigate the weather mechanisms underlying this extreme rainstorm in Jiangxi. By examining detailed observational data, the mesoscale weather characteristics and environmental conditions of the event can be obtained. These findings offer valuable insights for future weather forecasting and warnings. It was observed that after the Huanghuai cyclone moved eastward into the sea, the cold air on its western side shifted northward and converged with the warm, moisture-laden air mass in Hunan and Jiangxi provinces. This convergence of air masses triggered the heavy rainstorm event. The peak precipitation period occurred from midnight on May 5 to 0800 BJT on May 6. Concerning the macroscopic precipitation characteristics, multiple mesoscale convective systems (MCSs) originated in Hunan during this period and progressed eastward along the shear line toward the central part of Jiangxi. As for the microscopic precipitation features, the total precipitation amount was closely linked to the duration of heavy rain droplets. The rainfall distribution in the raindrop spectrum also served as a valuable reference for understanding the persistence and size of precipitation. The temporal pattern of the combined reflectivity echo along 27.5° N indicated that from 2000 BJT on May 5 to the early morning of May 6, there was a rapid development of a weaker MCS after passing through the Luoxiao Mountains. This development resulted in a "train effect" in the central region of Jiangxi. The presence of a 200 hPa divergence area, high vertical ascent rate, and abundant water vapor contributed to the formation of a narrow area of heavy rainstorms in central Jiangxi. Additionally, the falling area of heavy rain coincided with the front of the 500 hPa low trough. In the northern part of Jiangxi, the occurrence of heavy precipitation was influenced by the equivalent temperature front area. Favorable conditions, including water vapor, dynamics, and thermal factors, further supported the occurrence of heavy precipitation.

Keywords: heavy rainstorm; raindrop spectrum; Jiangxi Province; train effect

check for updates

Citation: Xiao, A.; Shan, J.; Chen, H.; Bao, H.; Xia, H.; Li, Z.; Liu, X. Mesoscale Characteristics of Exceptionally Heavy Rainfall during 4–6 May 2023 in Jiangxi, China. *Atmosphere* **2023**, *14*, 1735. https://doi.org/10.3390/atmos14121735

Academic Editor: Alexander V. Chernokulsky

Received: 22 October 2023
Revised: 20 November 2023
Accepted: 23 November 2023
Published: 25 November 2023

1. Introduction

Extreme rainstorms (heavy rainfall exceeding the historical maximum in 24 h) and heavy rainfall (total precipitation $\geq$ 50 mm$\cdot$day^{-1}) frequently lead to severe natural disasters such as landslides, debris flows, and flash floods, significantly endangering lives and property [1,2]. This gives rise to secondary meteorological disasters such as mountain torrents, mudslides, and geological hazards, with nighttime incidents posing the greatest risk to lives and property [3]. Rainstorms constitute the most critical meteorological hazard in Jiangxi, China [4]. Against the backdrop of global warming [5], both the frequency of rainstorms and the proportion of short-term heavy precipitation are increasing in Jiangxi, China [6,7]. Studies indicate that in Jiangxi during May, the occurrence of short-term heavy precipitation is more pronounced at night than during the day [8].

The primary flood season in Jiangxi spans from April to August. From April to mid-May, the southern regions of Jiangxi experience a higher incidence of heavy rainfall due to the pre-flood season in South China [9,10]. As May progresses into July, in tandem with the onset of the monsoon season and the northward shift of the subtropical high ridge line, the central and northern regions of Jiangxi progressively enter this phase, witnessing a rapid increase in rainstorm events. Notably, the most pronounced regional heavy rain events in Jiangxi typically occur during this period [11]. This is primarily attributed to Jiangxi's location within a subtropical monsoon climate zone, where there is abundant water vapor supply during this timeframe [12,13]. Nevertheless, in early May, the summer monsoon has yet to set in, resulting in a relative scarcity of water vapor in Jiangxi. Consequently, the energy conditions are suboptimal, making regional extremely heavy rainfall events relatively uncommon.

The occurrence of heavy rainfall necessitates three key elements: adequate water vapor supply [12,13], conducive dynamic uplift conditions, and prolonged precipitation duration [14]. Regarding water vapor supply, the role of low-level jet streams is crucial, as they establish an atmospheric channel for long-distance water vapor transport from low-latitude oceans to middle and high latitudes, providing essential conditions for heavy rainfall [15]. Additionally, rainstorms are typically closely tied to changes in meso-α-scale or synoptic-scale systems [16], such as the westward extension and northward shift of the western Pacific subtropical high [17,18], the northward movement of typhoons [19,20], and the development of synoptic-scale vortices and cyclones [21,22]. Furthermore, the development of meso-β-scale or meso-γ-scale convective systems during heavy rainfall often leads to short-term heavy rainfall [23–25]. Consequently, significant rainfall frequently arises from multi-scale interactions [26].

Conglomerates of convective storms are often organized on the mesoscale, behaving as long-lived ($\geq$3 h), discrete entities called mesoscale convective systems (MCSs). A specific subset of MCSs is known as mesoscale convective complexes (MCCs) [27]. Parker and Johnson identified and described the governing dynamics of three modes of linear MCSs as trailing stratiform (TS, a series of intense reflectivity cells solidly connected by an echo of more moderate intensity), leading stratiform (LS, a linear MCS whose stratiform precipitation is predominantly located in advance of a convective line), and parallel stratiform (PL, a linear MCS with a convective line and parallel stratiform precipitation). LS MCSs typically move more slowly than the other modes and thus may be more conducive to extreme rainfall and flash flooding [28].

Huang introduced the concept of a "warm-sector rainstorm" based on previous heavy rainfall occurrences during the flood season in South China [29]. Studies have indicated that this type of rainstorm is characterized by high intensity, a relatively concentrated period of precipitation, limited geographical range, and abrupt onset [30]. Many researchers in North China [31,32], Southwest China [33,34], Northwest China [35], Northeast China [36], and the Yangtze River Basin [37,38] have conducted numerous analyses of warm-sector rainstorm cases, contributing to extensive research progress.

Jiangxi Province is situated in the central part of South China (Figure 1a). An extremely regional warm-sector heavy rainfall event occurred in Jiangxi, China from 4 to 6 May, 2023. Owing to the warm and moisture-laden airflow transported by easterly winds, warm-sector rainstorms in Jiangxi province can result in substantial local precipitation and even significant losses. Instances of extremely heavy rainfall in Jiangxi caused by the warm zone in front of the trough in early May are relatively infrequent; hence, observation, analysis, and mechanistic research for this type of weather are not commonplace. This study not only investigated the observed data of this event based on minute-level observations and high-spatial-temporal-resolution raindrop spectrum data but also aimed to identify into the weather mechanisms of the warm-region storm in front of the trough. These research findings can offer technical support for weather forecasting in the future.

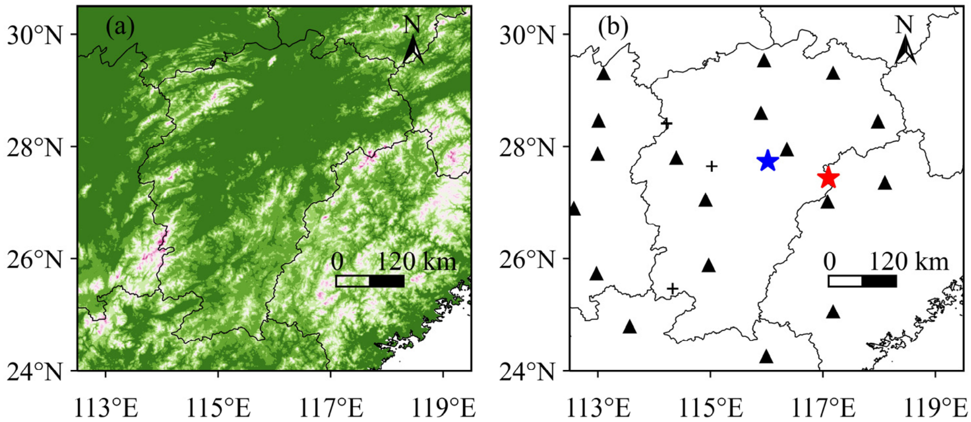

Figure 1. (**a**) Topography of Jiangxi Province and (**b**) ground observation stations in Jiangxi Province and its surrounding areas ("▲" represents meteorological radar stations, "+" represents precipitation centers in three stages, and blue and red five-pointed stars represent national stations and regional stations with the largest accumulated precipitation, respectively).

2. Dataset Introduction

The research utilized various datasets, including ground-based observation data, temperature of black body (TBB) data from the Fengyun-4A (FY-4A) satellite (provided by the National Satellite Meteorological Center of the CMA (China Meteorological Administration) at a resolution of 4 km $\times$ 4 km), radar data (at a resolution of 1 km $\times$ 1 km, Figure 1b), ERA5 global reanalysis data, and CLDAS (CMA Land Data Assimilation System) grid data (at a resolution of 5 km $\times$ 5 km) from the National Information Center of the China Meteorological Administration [39]. Additionally, raindrop data from Congren National Station (the location of blue five-pointed star in Figure 1b) and meteorological elements from 2557 automatic stations, made available by the Jiangxi Meteorological Data Center, were employed in this study. According to statistics, when the TBB of the MCS is less than -52 °C, the system is often accompanied by strong convective weather [40]. Radar echo intensity of short-duration heavy precipitation can exceed 40 dBZ, and radar echoes of some heavy rainfall can exceed 55 dbz [41].

The TBB data from the Fengyun-4A satellite represent full-disk 4KM-L1 data derived from the original packet data of the scanning imaging radiometer in the 13th channel (12 μm) following quality assurance, geolocation, and radiometric calibration. These data are characterized by a horizontal resolution of 4 km. The radar data employed in this research represent the combined reflectivity puzzle sourced from the National Information Center. The radar's location is depicted in Figure 1b. The spatiotemporal resolutions of the ERA5 reanalysis data are 0.25° $\times$ 0.25° and 1 h across 37 layers vertically [42]. This dataset is available at https://cds.climate.copernicus.eu/cdsapp#!/search?type=dataset&text=ERA5 (accessed on 15–16 November 2023). The raindrop spectrum data originated from the raindrop spectrometer at Chongren (116.05° E, 27.7667° N) National Meteorological Observatory, with a temporal resolution of 1 min.

In this paper, CLDAS data are used to calculate accumulated precipitation during the precipitation progress (see Figure 2). The CLDAS land surface data assimilation products are developed by using the techniques of multi-grid variability, spatial grid splicing, and discrete longitudinal short-wave radiation inversion with multi-land model ensemble simulation technology. Compared with other similar products in the world, the CLDAS series of land surface fusion analysis products have higher temporal and spatial resolution and quality in the Chinese region, and the spatial and temporal distribution characteristics are more accurate and reasonable.

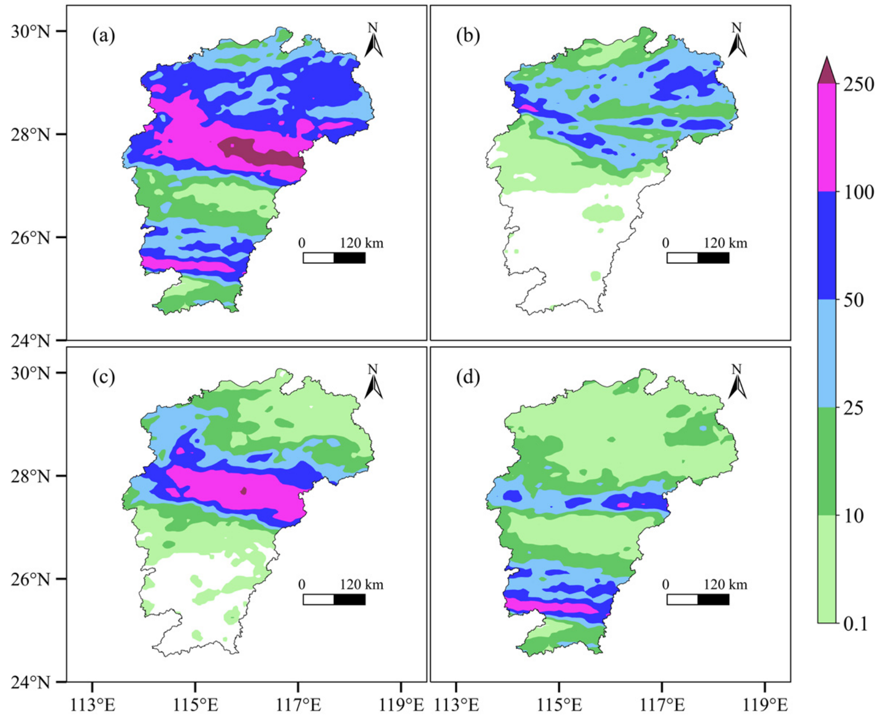

Figure 2. Accumulated rainfall (unit: mm) in Jiangxi Province from (**a**) 2000 BJT on 4 May to 2000 BJT on 6 May; (**b**) 2000 BJT on 4 May to 0800 BJT on 5 May; (**c**) 0800 BJT on 5 May to 0800 BJT on 6 May; and (**d**) 0800 BJT to 2000 BJT 6 May 2023.

The raindrop spectrometer model, a Parsivel excited spectrometer, was integrated within the Huachuang DSG4 precipitation phenomenon instrument. This one-dimensional laser raindrop spectrometer is capable of simultaneous measurement of particle falling velocity and diameter [43]. The recorded data comprised 32 diameter channels and 32 velocity channels within the raindrop spectrum. Raindrops falling within the measurable range exhibited diameters ranging from 0.125 to 26.0 mm, with falling velocities spanning from 0.1 to 22.4 m·s^{-1}, over a data collection interval of 1 min. Because of potential observational errors in raindrop spectrum data, it was imperative to implement data quality control measures. This involved excluding the initial two scale files and revised data featuring raindrop diameters exceeding 6 mm. Furthermore, samples with particle numbers (N) < 10 and rain intensity (R) < 0.1 mm·h^{-1} (primarily instrument noise) were omitted. Finally, data points where the observed velocity deviated more than 60% from the empirically calculated value based on the relationship V (D) = 9.65 − 10.3 exp (−0.6 D) between particle diameter (D) and maximum velocity (V) were also eliminated [44].

Consequently, it was crucial to convert the observed data into raindrop concentration per unit volume and scale interval.

$$N(D_i) = \sum_{i=1}^{32} \frac{n_{ij}}{A \Delta t V_j \Delta D_i} \tag{1}$$

where n_{ij} denotes the number of raindrops within the i-th scale interval with falling speeds within the j-th speed interval, A represents the sampling area of the instrument (unit: m^2), Δt is the sampling time interval (unit: s), D_i and ΔD_i signify the central diameter of the i-th scale interval and the scale interval of the interval (unit: mm), V_j stands for the central speed of the j-th speed interval (unit: m·s^{-1}), and N(Di) signifies the number of raindrops in the unit volume and scale interval of D_i and D_i + ΔD_i (unit: mm^{-1}·m^{-3}).

The formulas for calculating the mass-weighted average diameter (D_m) and rainwater content (Z) (unit: $mm^6 \cdot m^{-3}$) from raindrop spectrum data are as follows:

$$D_m = \frac{\sum_{i=1}^{32} D_i^4 N(D_i) \Delta D_i}{\sum_{i=1}^{32} D_i^3 N(D_i) \Delta D_i} \tag{2}$$

$$Z = \sum_{i=1}^{32} D_i^6 N(D_i) \Delta D_i \tag{3}$$

3. Overview of the Rainfall Event

An exceptionally large-scale heavy rainfall event occurred in Jiangxi from 2000 BJT (Beijing time, the same as below) on 4 May to 2000 BJT on 6 May 2023 (Figure 2a). The maximum areal rainfall reached 168.4 mm in the Fuhe River Basin, with the highest 24 h rainfall of 417.1 mm recorded at Feiyuan station (FY, 117.0986° E, 27.4389° N), Lichuan County. The entire precipitation event could be divided into three stages based on the influencing weather system and the location of the rainstorm area. These stages were from 2000 BJT on May 4 to 0800 BJT on May 5 (referred to as “Stage-1”, Figure 2b), from 0800 BJT on May 5 to 0800 BJT on May 6 (referred to as “Stage-2”, Figure 2c), and from 0800 to 2000 BJT on May 6 (referred to as “Stage-3”, Figure 2d).

During Stage 1, the primary precipitation area was situated in the northern part of northern Jiangxi. There were 11 national stations and 264 regional stations reporting 12 h precipitation levels $\geq$ 50 mm, among which 1 national station and 12 regional stations recorded 12 h precipitation levels $\geq$ 100 mm. These were mainly concentrated in northwestern Jiangxi. In Stage 2, the main precipitation area was located between 27° and 29° N. A total of 21 national stations and 442 regional stations reported 12 h precipitation levels $\geq$ 50 mm. The area also experienced the highest rainfall across the three stages. There were 8 national stations and 146 regional stations with 12 h precipitation levels $\geq$100 mm, with the main precipitation period occurring from 2000 BJT on May 5 to 0600 BJT on 6 May. In Stage 3, the primary precipitation area was primarily situated in a narrow region near 25.5° N. There were 10 national stations and 258 regional stations with 12 h precipitation levels $\geq$50 mm, among which 1 national station and 57 regional stations recorded 12 h precipitation levels $\geq$100 mm. The main precipitation affected southwestern Jiangxi from west to east from 0800 to 2000 BJT on May 6. At 0750 BJT on 6 May 2023, it was also observed that there were two centers of heavy precipitation areas in this torrential rain event, with areas exceeding 100 mm forming quasi-east–west narrow bands. In the second stage, the heavy rain areas were primarily located at 27–28° N, while those above 250 mm were slightly oriented southwest-northeast, with a north–south width of about 0.3° N, indicating a very narrow band. In the third stage, the heavy rain areas were mainly concentrated at 25.3–25.5° N.

To investigate the hourly rainfall patterns at stations during this precipitation event, this study examined the Stage 1 maximum rainfall regional station (Zengxi Village, ZX, 114.2217° E, 28.4131° N), the Stage 2 maximum rainfall regional station (Hongqiao Town, HQ, 115.0256° E, 27.6508° N), the Stage 3 maximum rainfall regional station (Dangping Tungsten Mine, DP, 114.3292° E, 25.4628° N), and the regional station with the highest cumulative rainfall over the entire event (Feiyuan Village, FY). As depicted in Figure 3, the primary rainfall period in ZX extended from 2300 BJT on 4 May 2023 to 0400 BJT on 5 May 2023. Within this period, the maximum hourly rainfall intensity reached 50.5 mm. In stage 2, HQ recorded the highest hourly rainfall in this event, accumulating 117.6 mm over 2 h. However, the heavy rainfall subsequently decreased. At FY station, the rain persisted from 0800 BJT on May 5 to 2000 BJT on 6 May 2023, resulting in a cumulative rainfall of 447.5 mm exceeding 36 h, surpassing historical records since the station’s establishment. Concurrently, HQ also experienced rainfall during this period, with the maximum hourly rainfall intensity only reaching 23.4 mm, and the convection was comparably weak. DP station recorded the highest accumulated rainfall of 189.1 mm in Stage 3, with the maximum hourly rainfall intensity of 52.8 mm occurring at 1500 BJT on 6 May 2023. Therefore, precipitation convection was most intense during the day on May 5, while it was moderate during the nights of May 4 and May 6, with the latter featuring the highest cumulative precipitation but relatively weak convection.

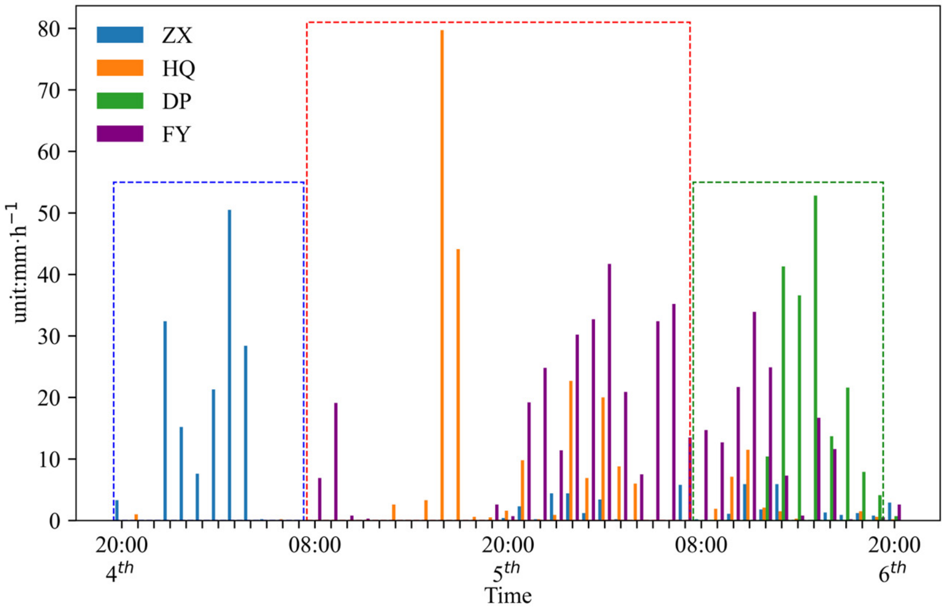

Figure 3. Time series of hourly rainfall at ZX, HQ, DP, and FY stations from 2000 BJT on May 4 to 2000 BJT on 6 May 2022. "ZX", "HQ", "DP", and "FY" denote Zengxi Village, Hongqiao Town, Dangping Tungsten Mine, and Feiyuan Village regional weather station, respectively. The blue, red, and green dashed-line boxes represent Stage 1, Stage 2, and Stage 3, respectively.

4. Macroscopic and Microscopic Characteristics of Rainfall

Based on the foregoing analysis, it is evident that the second stage exhibited the longest duration of rainfall and the highest cumulative precipitation. To further elucidate, this study examined the macroscopic features of heavy rainfall using raindrop spectrum data from the Chongren National Meteorological Station (CR). This station experienced an isolated short-term heavy precipitation event at 0700 (35.6 mm·h^{-1}) BJT on 5 May 2023. Another short-term heavy precipitation event occurred at night and extended from 1800 BJT on May 5 to 0600 BJT on 6 May 2023, resulting in a cumulative rainfall of 230.3 mm over 12 h (Figure 4a). Examining the time series of radar composite reflectivity (Figure 4b), it was observed that CR station's combined reflectivity was around 15 dBZ at 2000 BJT on 4 May 2023, persisting until 0354 on May 5. Starting at 0400 BJT, the reflectivity began to rise, reaching 32.5 dBZ at 0524-0624 BJT and then rapidly declining from 0700 to 0754 BJT on 5 May 2023, in line with the short-term heavy precipitation at 0700 BJT at CR station. The composite reflectivity exceeded 20 dBZ at 1430 BJT on May 5 over CR station, although no corresponding ground-level precipitation was recorded. After 1700 BJT, the composite reflectivity of the CR station surged and held steady between 40 and 50 dBZ. These signified continuous and strong echoes impacting the CR station, aligning with the period of heaviest precipitation. After 0500 BJT on 6 May 2023, the composite reflectivity began to fluctuate notably yet remained predominantly robust, ranging between 25 and 35 dBZ. However, precipitation during this period was comparatively subdued, resulting in lower echo precipitation. Between 1700 and 1900 BJT on May 6, the echo dropped to approximately 10–20 dBZ, indicating the event was nearing its end.

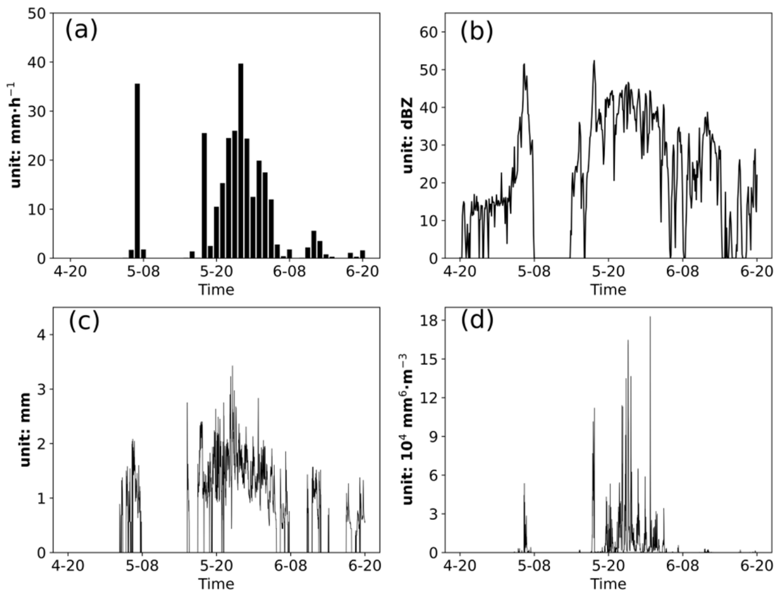

Figure 4. Time series of (**a**) hourly rainfall, (**b**) 6 min radar composite reflectivity, (**c**) 1 min weighted average diameter of raindrop spectrum mass, and (**d**) 1 min raindrop spectrum raindrop content at CR station from 2000 BJT on May 4 to 2000 BJT on 6 May 2023.

Analyzing the macroscopic characteristics of precipitation, it is evident that while radar echo composite reflectivity provided valuable insight into the evolution of the heavy rainfall, there were instances where moderate-intensity composite reflectivity echoes did not correspond to significant precipitation in the area. Therefore, a microscopic analysis of rainfall characteristics became imperative. As illustrated in the mass-weighted average diameter of the raindrop spectrum, between 0600 and 0800 BJT on 5 May 2023, raindrop diameters ranged from 0.56 to 2.08 mm, with a median of 1.1 mm, indicating relatively small-sized raindrops. From 1517 to 1534 BJT, CR station experienced raindrops with a maximum mass-weighted average diameter of 2.75 mm, but due to the brief duration (18 min), only 1.4 mm of precipitation accumulated (Figure 4c). Continuous precipitation at CR station commenced at 1659 BJT on May 5, with raindrops exhibiting generally larger diameters. The maximum diameter reached 3.4 mm, with a median of 1.4 mm, indicating higher precipitation efficiency. By 0800 BJT on May 6, the mass-weighted average diameter began to notably decrease, signifying a reduction in the number of large raindrops, consistent with the actual rainfall. In contrast to radar composite reflectivity, raindrop content demonstrated a notably better correspondence with precipitation. Additionally, the correlation between raindrop content and heavy precipitation was also stronger. At 0624 BJT on 5 May 2023, raindrop content peaked at 5.36×10^4 mm^6·m^{-3}. After 0800 BJT on May 6 (Figure 4d), while the radar composite reflectivity remained at 25–35 dBZ, rainwater content significantly dwindled, resulting in minimal precipitation. Consequently, rainwater content derived from the raindrop spectrum holds crucial significance in understanding the persistence and cumulative amount of rainfall.

5. Analysis of Heavy Rainfall

5.1. Analysis of Circulation Situation

Transitioning into early May, the East Asian monsoon had not yet manifested, and the western Pacific subtropical high remained stationary, failing to extend westward and northward. Consequently, South China progressively entered its rainy season. At 500 hPa, the high-latitude circulation in Asia primarily consisted of two troughs and one ridge. One trough was positioned in northern Xinjiang, while the other was near the Okhotsk Sea by 2000 BJT on 4 May 2023 (Figure 5a). Between these troughs lay a wide expanse of weak high-pressure ridges. In the mid-latitudes, a low trough moved eastward toward the

Huanghuai Basin. The subtropical high in lower latitudes remained stable with minimal movement, maintaining a peripheral 584 dagpm around 24.5° N throughout the entire rainstorm process. At 850 hPa, the Huanghuai cyclone shifted eastward from Henan to Shandong, ultimately making its way into the Bohai Sea. The northerly airflow on its western side descended southward to central and eastern Hubei, while the southwest airflow around the subtropical high affected the Yangtze River basin (Figure 6a). The first phase of precipitation occurred in Northern Jiangxi, influenced by the lower-level shear of the Huanghuai cyclone, along with the presence of strong southwest warm and moist air. By 2000 BJT on 5 May 2023, the radiality of the 500 hPa mid-latitude low trough deepened further as it shifted slightly eastward, with the trough base extending southward to 32° N. This setup facilitated the guidance of cold air behind the trough, influencing the middle and lower reaches of the Yangtze River (Figure 5b). A short-range short-wave trough moved from west to east in Jiangxi, bringing good dynamic conditions for heavy rainfall (see Section 5.3). At 850 hPa, the Huanghuai cyclone's forward motion slowed upon entering the sea. The northerly airflow on its western flank intensified the southward movement of cold air, causing the wind shear line in the Yangtze River basin to advance over the Yangtze River (Figure 6b). Concurrently, the northerly airflow on the western side of the Huanghuai cyclone transitioned into a northeasterly jet stream, merging with a similar stream from northeastern China. This merged flow through Shandong, Henan, and Hubei converged with the southwesterly warm and humid jet stream in Guangxi around the subtropical high. Under suitable thermodynamic and dynamic conditions, multiple mesoscale convective systems (MCSs) [45] formed along the shear line and moved eastward into Jiangxi. By 0800 BJT on 6 May 2023, the shallow trough gradually shifted eastward and pressed southward at 500 hPa (Figure 5c), with the northeasterly jet stream further enhancing the warm conditions over southern Jiangxi. The infusion of cold air into Hunan led to the formation of a meso-α-scale MCS in Hunan, which then advanced eastward into Jiangxi. This MCS brought heavy rainfall to Ganzhou, Jiangxi, on May 6 (Figure 6c). By 2000 BJT on May 6, the northeast jet stream essentially blanketed the entirety of Jiangxi (Figure 5d), causing heavy precipitation to shift toward Fujian Province and marking the conclusion of the large-scale heavy rain event in Jiangxi (Figure 6d).

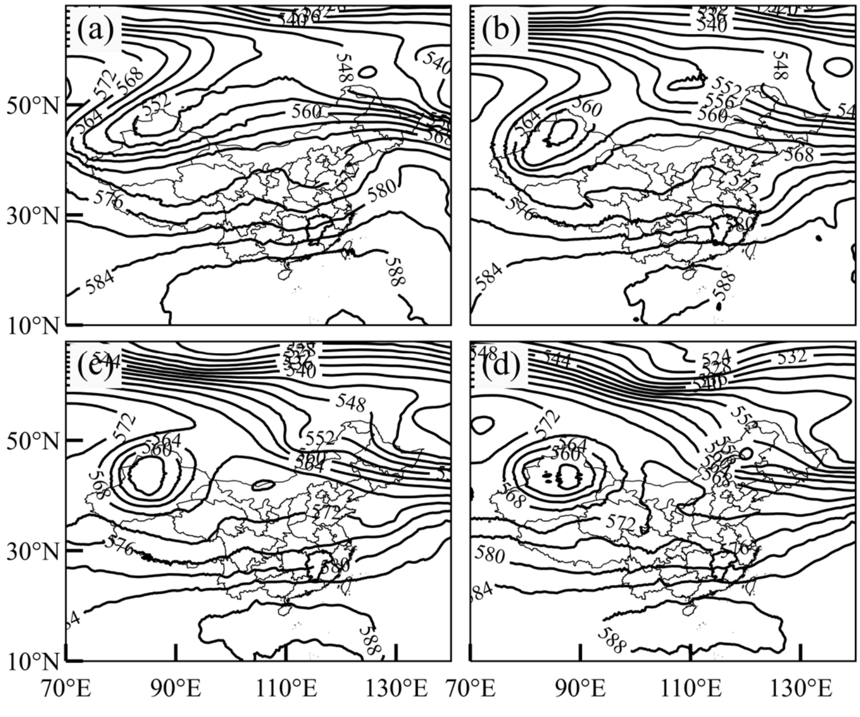

Figure 5. Geopotential height (unit: dagpm) at 500 hPa at (**a**) 2000 BJT on May 4, (**b**) 2000 BJT on May 5, (**c**) 0800 BJT on May 6, and (**d**) 2000 BJT on 6 May 2023.

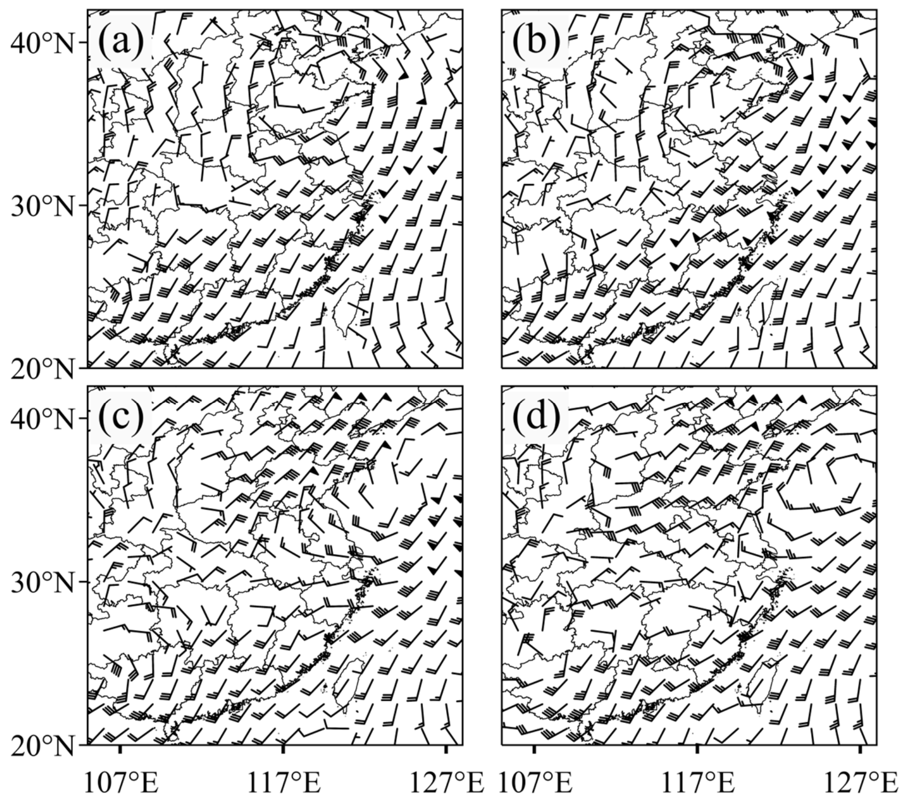

Figure 6. Wind (850 hPa; unit: m s^{-1}) at (**a**) 2000 BJT on May 4, (**b**) 0800 BJT on May 5, (**c**) 2000 BJT on May 5, and (**d**) 0800 BJT on 6 May 2023.

In the wake of cold air influx and robust convective activity, the temperatures at 2 m above ground level (T2m) in Hunan dropped, creating a widespread cold-pool system on 6 May 2023. This intensified the surface temperature gradient from Hunan to Jiangxi, aiding the further eastward progression of the MCS from Hunan into Jiangxi. From 0400 to 0800 BJT (Figure 7a,b), the T2m in most parts of Hunan had dropped to 18~22 °C, a widespread cold-pool system triggered widespread strong convective weather in Hunan (A_4 in Figure 8g, MCS-E and MCS-F in Figure 9h), and T2m in southern Jiangxi reached 26~28 °C, with an obvious temperature gradient between the two provinces. At 1400 BJT, the T2m in southern Hunan dropped to 18~21 °C, and the temperature gradient between the two provinces slightly decreased (Figure 7c). At 1800 BJT, the temperature gradient between the two provinces decreased to 2~4 °C (Figure 7d), and the precipitation process in southern Jiangxi also tended to end.

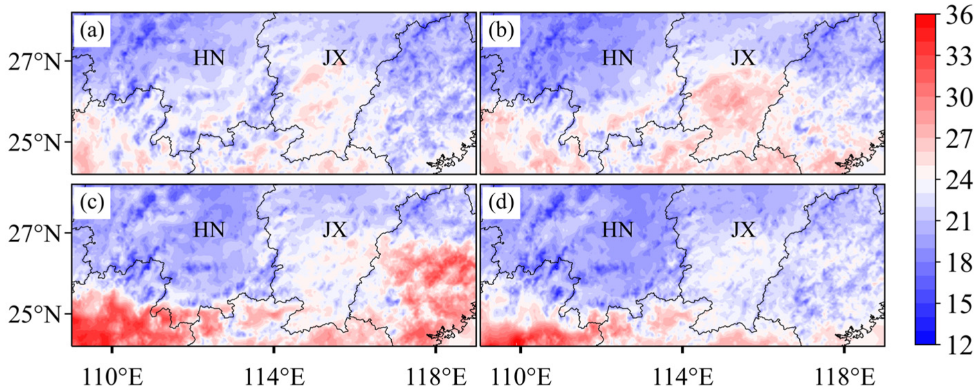

Figure 7. The temperature at 2 m above ground level (unit: °C) at (**a**) 0400 BJT, (**b**) 0800 BJT, (**c**) 1400 BJT, and (**d**) 1800 BJT on 6 May 2023. "HN" and "JX" denote Hunan and Jiangxi province, respectively.

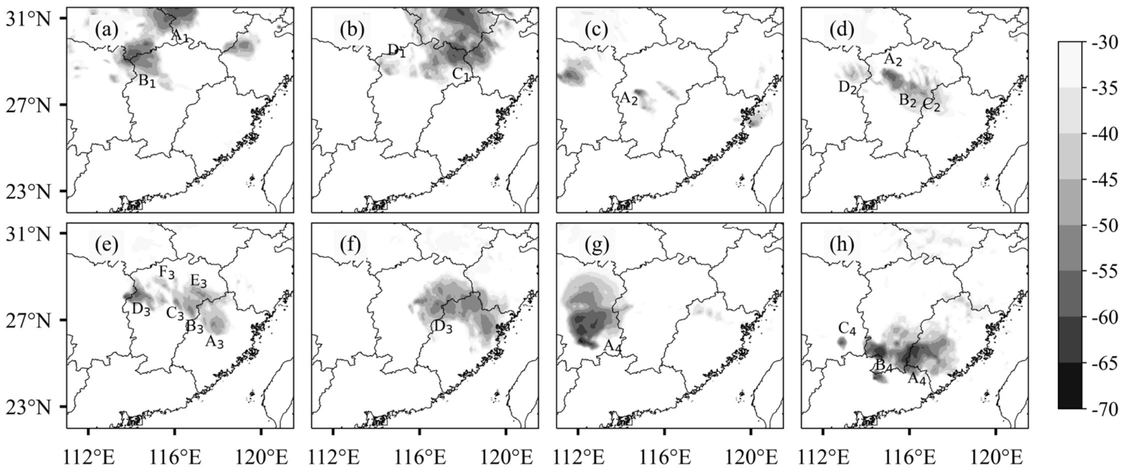

Figure 8. TBB of FY−4A (shaded, unit: °C) at (**a**) 2000 BJT on May 4, (**b**) 0200 BJT on May 5, (**c**) 1500 BJT on May 5, (**d**) 1800 BJT on May 5, (**e**) 2000 BJT on May 5, (**f**) 0000 BJT on May 6, (**g**) 0800 BJT on May 6, and (**h**) 1400 BJT on 6 May 2023.

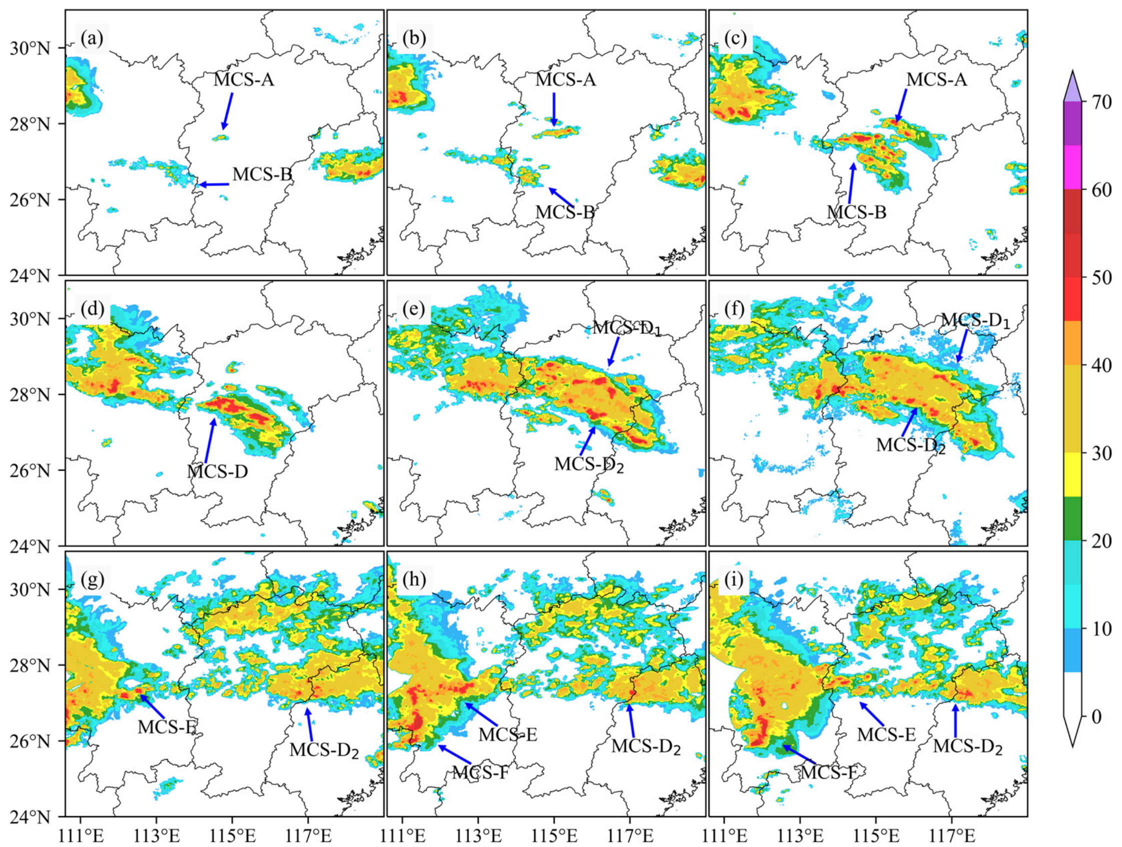

Figure 9. Radar composite reflectivity echoes over Jiangxi and surrounding provinces at (**a**) 1200, (**b**) 1300, (**c**) 1500, (**d**) 1600, (**e**) 1900, and (**f**) 2000 BJT on May 5 and (**g**) 0600, (**h**) 0700, and (**i**) 0800 BJT on 6 May 2023.

The evolution characteristics of mesoscale convective systems (MCSs) in the three stages can be clearly distinguished from FY-4A satellite cloud images. At 2000 on May 4, during the rapid eastward movement and northward lifting of the Huanghuai cyclone, the tail cloud system A_1 extended to approximately 30° N. In the northern part of Hunan Province, an MCS (B_1) moved rapidly eastward toward the vicinity of Mufu Mountain in northwest Jiangxi Province and gradually strengthened (Figure 8a). At 2100 BJT, A_1 and B_1

merged into C_1 and continued to move rapidly eastward, bringing significant precipitation to the area north of 29° N in Jiangxi Province (data not shown). At 0200 BJT on May 5, C_1 had moved to the northeast of Jiangxi Province (Figure 8b), and its impact on Jiangxi was diminishing. A new MCS (D_1) had formed in the northeast of Hunan Province and was moving eastward toward the northwest of Jiangxi Province. Its TBB of ≤ -50 °C resulted in short-term heavy precipitation of 50.5 mm h^{-1} at ZX station. The MCS then gradually and rapidly moved eastward out of Jiangxi Province, bringing substantial precipitation along 28° N (as depicted, but not shown in full). At 1500 BJT on May 5, two new MCSs appeared in the central region of Jiangxi Province. The northern MCS dissipated within 2 h, while the southern MCS (A_2) rapidly developed northward (Figure 8c). By 1800 BJT, it had evolved into a meso-β-scale system in the northwest of Jiangxi Province, with a minimum TBB of approximately −59 °C. Additionally, there were new MCSs (B_2, C_2) in the southeast of A_2. Another MCS (D_2) emerged in the eastern part of Hunan Province to the west of A_2. These MCSs not only brought intense, short-term heavy precipitation locally but also merged into a linear MCS. The direction of movement shifted from north–south along the short axis on May 5 to west–east along the long axis at night (Figure 8d). At 2000 BJT on May 5, around the linear MCSs, several other MCSs (C_3, E_3, F_3) with smaller influence ranges and slightly higher TBB values were successively triggered of approximately −40 to −45 °C. D_3 had a relatively low TBB, reaching −60 °C at its lowest. The central and eastern areas of Jiangxi were continuously affected by the "train effect" [46] of linear MCSs (Figure 8e), resulting in heavy precipitation in Stage 3. At 0000 BJT on May 6, D_3 shifted from western Jiangxi to eastern Jiangxi, and a few newly triggered MCSs appeared on its west side. However, their lifespan was short, and their influence range was limited (Figure 8f). At 0800 BJT on May 6, all the main MCSs in Stage 3 moved eastward. A_4 quickly advanced to the eastern part of southern Jiangxi, and the newly triggered MCSs (B_4, C_4) at the rear gradually moved eastward along 25° N (Figure 8g), forming the second "train effect" in this process. After C_4 moved eastward out of Jiangxi Province, the rainstorm process in Ganzhou gradually concluded (Figure 8h). Although the "train effect" of MCSs such as A4, B4, and C_4 in this stage was not as prolonged as in the third stage, the TBB of many MCS cloud systems was lower than −65 °C, with the lowest reaching −70 °C. Therefore, the precipitation intensity in this stage was relatively high, forming the second heavy rain belt in this torrential rain process.

5.2. Evolution Characteristics of Radar Echo

The precipitation in the second stage of this heavy rainfall was the most intense. At 1200 (noon) BJT on 5 May 2023, primary convection formed in the central part of Jiangxi (around 113.5° E, 27.7° N). Simultaneously, a weak echo moved eastward from the eastern part of Hunan and entered Jiangxi through the Luoxiao Mountains (Figure 9a). At 1300 BJT, the primary convection began to develop into MCS-A, with the strongest combined reflectivity reaching 55 dBZ, and it dissipated around 1600 BJT. At 1300 BJT, the incoming echo from Hunan rapidly strengthened into MCS-B, propagating from southwest to northeast (Figure 9b,c) with a relatively slow speed. At 1600 BJT, the eastward-propagating MCS-C and the developed MCS-B gradually merged into a quasi-east–west linear echo, MCS-D (Figure 9d). At 1900 BJT, the echo split into two linear echoes (Figure 9e). Among them, the north echo, MCS-D1, propagated slightly northward and soon dissipated, while the south echo, MCS-D2, began to propagate eastward and became the main influencing echo in the second stage of the rainstorm. From 2000 BJT on May 5 to 0800 BJT on May 6, the vicinity of 27.5° N in Jiangxi was affected by the eastward movement of several MCSs, resulting in regional heavy rain and local heavy rain in the Fuhe River Basin (Figure 9f–i).

From the preceding analysis, it is evident that Hunan was influenced by cold air from the north, resulting in the birth of numerous MCSs. However, their intensity and influence range were relatively small. Once these systems entered Jiangxi, they tended to undergo rapid development or merge with existing strong echoes, thereby intensifying the echoes further. To delve deeper into this evolutionary characteristic, considering that the echoes on the night of May 5 mainly propagated in the zonal direction, this study makes a longitude–time profile of radar-combined reflectivity echoes along 27.5° N to investigate the zonal movement patterns of MCS (Figure 10a). If an MCS had been moving in a zonal direction, it would present as a straight line from lower left to upper right on the graph. The steeper the slope, the longer the duration of the MCS and the shorter the distance, thus indicating a slower eastward movement speed; conversely, a flatter slope signifies a faster pace. At 1400 BJT on May 5, specifically between 112 and 114° E, the combined reflectivity of most MCSs echoes measured below 20 dBZ, but this rapidly escalated to 40–50 dBZ in the area east of 113.5° E. This enhanced area of the echo aligned with the Luoxiao mountain range, with altitudes surpassing 1000 m. This topographic feature distinctly contributed to the forced uplift of the MCS. With the amplification of MCS-A, three individual MCS units (MCS-B, MCS-C, and MCS-D) were newly generated due to topographic uplift at 0000 BJT on May 6. Subsequently, all these echoes moved eastward, instigating a sustained "train effect" downstream. Moreover, between 114° and 115°E lies the Jitai Basin in Jiangxi, characterized by a lack of mountainous terrain. This area hosted numerous convective cells that were predominantly new due to the eastward expansion of the echoes. Additionally, examining the time–height profile of the reflectivity factor at CR station, this study observed that from 2000 BJT on May 5 to 0500 BJT on May 6, echoes above 40 dBZ were continuously affecting CR station, with a vertical distribution characterized by a low center of mass, indicating a typical continuous heavy precipitation echo feature (Figure 10b).

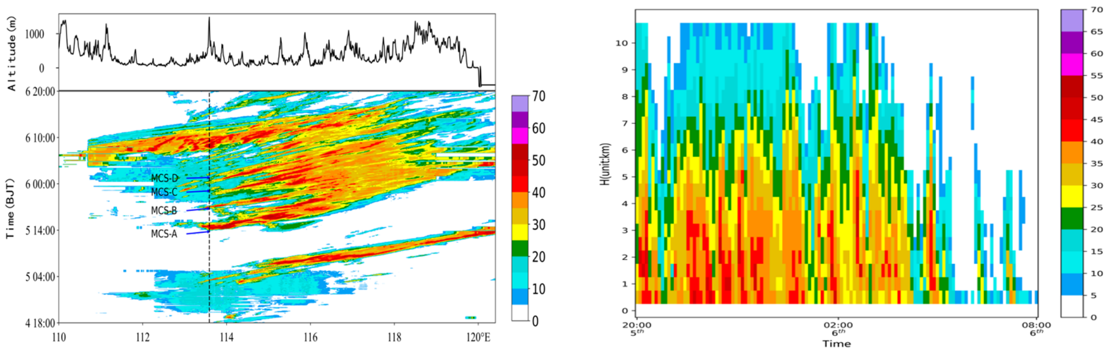

(**a**) (**b**)

Figure 10. (**a**) Time profile of the combined reflectivity echo along 27.5° N (unit: dBZ, the upper curve represents the altitude of the latitude terrain) and (**b**) time variation of the reflectivity factor height at Chongren National Station (unit: dBZ).

5.3. Analysis of Heavy Rainfall Area

Inspecting the precipitation distribution in Figure 1c,d, along with the radar echo features in Figure 9, it becomes apparent that in the second and third stages of heavy precipitation, the heavy rain belt was relatively narrow. On either side of this zone, there existed a significant precipitation gradient. What could be the possible explanation for this phenomenon? From the 200 hPa wind field at 2000 BJT on 5 May 2023, the results revealed that Jiangxi was predominantly influenced by westerly and northwest winds. The divergence area was situated in Fuzhou, Jiangxi Province. North of Fuzhou (beyond 28° N) lay a large convergence area, while the southern region experienced weaker convergence and divergence (Figure 11a). Likewise, examining the composite map of wind and vertical velocity in the v-direction along 116° E at the same time (Figure 11b), the results revealed that in the lower layer south of 27° N, a consistent southerly wind prevailed. Between 27° and 27.8° N, an updraft was evident. This updraft extended up to 200 hPa before shifting to a northerly direction. The northerly winds below 900 hPa north of 28° N were relatively shallow, indicating the onset of weak cold air entering the northwestern part of Jiangxi. This layer was marked by a weak southerly wind but with insufficient convergence of water vapor flux, and the specific humidity at 925 hPa was only 12 $g\cdot kg^{1}$, which was lower than the average of the specific humidity of May rainstorm days in Jiangxi [47]. Consequently, precipitation in this stage was predominantly concentrated in Fuzhou, and the specific humidity was 16 g·kg^1 at 925 hPa, which is relatively uncommon in early May in Jiangxi. By 0000 BJT on May 6, a short-wave trough was moving from west to east near 28.5° N. This trough creates a discernible area of divergent motion in its front, roughly spanning from 27.5° to 28.5° N. Coupled with lower-layer convergence (Figure 11c), heavy precipitation most likely occurred in this area. North of 28.5° N, another expansive convergence area existed. However, due to poor water vapor conditions similar to those in Figure 9b, heavy precipitation did not occur here. As the short-wave trough progressively moved out of Jiangxi, the 850 hPa equivalent potential temperature map at 0600 BJT on May 6 (Figure 11d) clearly illustrates the formation of a broad equivalent potential temperature dense zone from southwestern Hunan to northeastern Jiangxi as cold air infiltrated from the north. In northern Hunan, the lowest equivalent potential temperature was 324 K, while the highest in the south was 350 K. In Jiangxi Province, it ranged between 346 K and 348 K. Consequently, an evident intersection of cold and warm air masses occurred in Hunan, making conditions conducive to the development of a robust MCS that subsequently moved eastward, influencing Jiangxi. The MCS affecting Ganzhou during the day on May 6 was a direct result of this scenario. Simultaneously, a low equivalent potential temperature center in northeastern Jiangxi continued to expand as the cold air permeated this region. Within 2–3 h, the equivalent potential temperature gradient on both sides of the area along the Yangtze River tended to dissipate, and the dense zone of equivalent potential temperature shifted southward to central Jiangxi, effectively concluding the second stage of precipitation in Jiangxi.

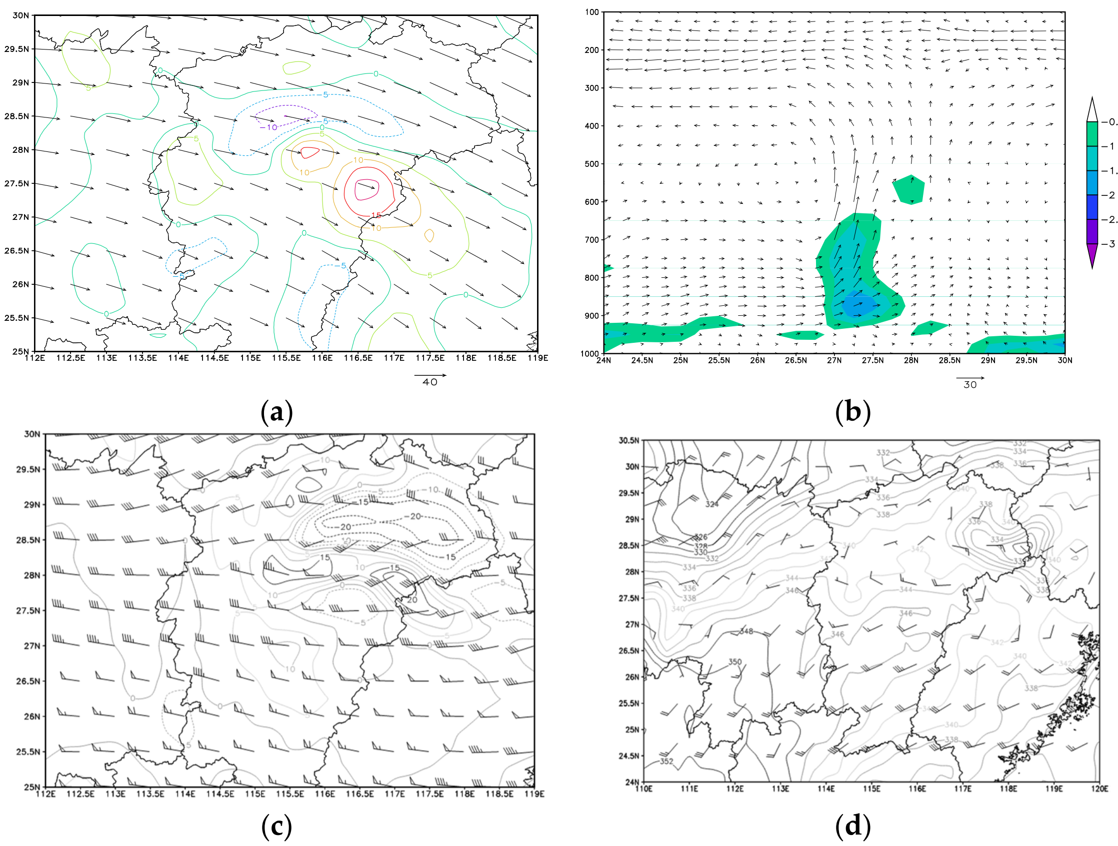

Figure 11. (**a**) Wind fields (vector, unit: m·s^{-1}) and divergence (lines, $\times10^{-5}$ s^{-1}) at 200 hPa at 2000 BJT on 5 May 2023, (**b**) latitude–height profile along 116° E (unit: m·s^{-1}) at 2000 BJT on 5 May 2023, (**c**) wind fields (vector, unit: m·s^{-1}) and divergence (lines, $\times10^{-5}$ s^{-1}) at 200 hPa at 0000 BJT on 6 May 2023, and (**d**) wind fields at 500 hPa (barbs, unit: m·s^{-1}) and the equivalent potential temperature at 850 hPa (lines, unit: K) at 0600 BJT on May 6.

6. Conclusions

In this study, the regional heavy rainfall in Jiangxi Province was analyzed from May 4 to 6, 2023, utilizing conventional high-altitude ground observation data, ground regional encrypted observation data, FY-4A satellite cloud image TBB data, ERA5 reanalysis data, and Parsivel laser raindrop spectrum data provided by the Huachuang DSG4 precipitation phenomenon instrument. Additionally, this study evaluated the forecast results from various numerical forecasting products. The following conclusions can be drawn:

(1) By categorizing the precipitation process into three stages based on the timing and influencing systems, it is evident that the second stage yielded the highest cumulative precipitation. The primary influencing weather system during this process was the northern Huanghuai cyclone. After the cyclone moved into the sea, the northerly jet stream on its western flank penetrated Hunan and Jiangxi provinces through the Yangtze River, establishing a quasi-stationary front with the warm and humid airflow in the southern regions of the two provinces. This interaction led to sustained periods of heavy precipitation.

(2) Examining the macroscopic features of precipitation, while the combined reflectivity of radar echoes provided a better reflection of the evolving state of each heavy precipitation event, there exists a range of medium-intensity combined reflectivity where precipitation was not readily apparent. Delving into the microscopic characteristics of precipitation, cumulative precipitation demonstrated a strong correlation with the duration of heavy raindrops. Moreover, the raindrop spectrum's rainwater content served as a significant reference for both the duration and intensity of precipitation.

(3) The analysis reveals that several weak MCSs underwent rapid development after traversing the Luoxiao mountain range, giving rise to a "train effect" in the central part of Jiangxi. Factors such as the 200 hPa divergence area, substantial vertical updrafts, and ample moisture content contributed to the formation of a very narrow rainstorm area in central Jiangxi. Simultaneously, this rainstorm area was positioned ahead of the 500 hPa low trough, with the northern sector being influenced by the equivalent potential temperature front area in the northeast of Jiangxi. These conditions collectively created a favorable environment for heavy precipitation, incorporating considerations of moisture, dynamics, and thermal aspects.

Author Contributions: Conceptualization, A.X. and H.B.; methodology, J.S.; software, A.X., H.X. and Z.L.; formal analysis, A.X. and H.B.; writing—review and editing, A.X. and H.C.; data collection and curation, J.S.; supervision, H.X.; visualization, A.X., X.L. and H.X.; funding acquisition, A.X. All authors have read and agreed to the published version of the manuscript.

Funding: This study was jointly supported by the Innovation and Development Program of China Meteorological Administration (Grant No. CXFZ2021Z012), the Key Program (Grant No. 202202ybxm01, JX2023Z05) of the Jiangxi Meteorological Bureau, and the Weather Forecast Recovery Project of the China Meteorological Administration (Grant No. FPZJ2023-009).

Institutional Review Board Statement: Not applicable.

Informed Consent Statement: Not applicable.

Data Availability Statement: The data that support our research findings are available from the corresponding author on request. The data are not publicly available due to privacy restrictions.

Acknowledgments: We thank the National Meteorological Center of the China Meteorological Administration for the experimental data.

Conflicts of Interest: The authors declare no conflict of interest.

References

1. Gu, X.; Ye, L.; Xin, Q.; Zhang, C.; Zeng, F.; Nerantzaki, S.D.; Papalexiou, S.M. Extreme Precipitation in China: A Review on Statistical Methods and Applications. *Adv. Water Resour.* **2022**, *163*, 104144. [CrossRef]
2. Özdemir, E.T.; Yavuz, V.; Deniz, A.; Karan, H.; Kartal, M.; Kent, S. Squall line over Antalya: A case study of the events of 25 October 2014. *Weather* **2019**, *4*, S1–S6. [CrossRef]
3. Ren, Z.; Sang, Y.; Yang, M.; Wang, Y.; Shang, L. Progress of research on the methods for the early warning of mountain flash flood disasters. *Prog. Geogr.* **2023**, *42*, 185–196. (In Chinese) [CrossRef]
4. Ding, Y. The major advances and development process of the theory of heavy rainfalls in China. *Torr. Rain Dis.* **2019**, *38*, 395–406. (In Chinese)
5. Allen, M.; Ingram, W. Constraints on future changes in climate and the hydrologic cycle. *Nature* **2002**, *419*, 224–232. [CrossRef] [PubMed]
6. Wang, J.; Zhang, J.; Wu, T.; Zhong, M.; Wang, S.; Zhou, J.; Huang, X.; Han, F.; Wang, C. MCS Classification and Characteristic Analyses of Extreme Short Time Severe Rainfall in Hubei Province. *Meteorol. Mon.* **2019**, *45*, 931–944. (In Chinese)
7. He, X.; Hao, Y.; Qi, H.; Cui, C.; Qin, Y.; Yang, T.; Li, K.; Tang, J. Analysis of characteristics and causes of "8.12" extreme precipitation in Hubei Province. *Torr. Rain Dis.* **2023**, *42*, 13–23. (In Chinese)
8. Xiao, A.; Yin, X.; Liu, X. Temporal and spatial distribution characteristics of diurnal variation of precipitation in Jiangxi Province. *J. Arid Meteorol.* **2022**, *40*, 840–848. (In Chinese)
9. Chu, Q.; Wang, Q.; Feng, G. The Roles of Moisture Transports in Intraseasonal Precipitation during the Preflood Season over South China. *Int. J. Climatol.* **2019**, *40*, 2239–2252. [CrossRef]
10. Yuan, Y.; Ren, F.; Wang, Y.; Guo, Y.J. Analysis of the Precipitation Feature and General Circulation Anomaly during the Pre-Flood Season in South China in 2012. *Meteorol. Mon.* **2012**, *38*, 1247–1254.
11. Zhi, S.; Chen, J.; Bao, H. Mesoscale Characteristics Analysis of Rainstorm on the Edge of Subtropical High. *Meteorol. Mon.* **2015**, *41*, 1203–1214. (In Chinese)
12. Sampe, T.; Xie, S.P. Large-Scale Dynamics of the Meiyu-Baiu Rainband: Environmental Forcing by the Westerly Jet. *J. Clim.* **2010**, *23*, 113–134. [CrossRef]
13. Chen, Y.; Duan, J.; Qian, Y.; Xu, D.; Guo, Y. Analysis on Water Vapor Transport Effect During Meiyu Period in Zhejiang Caused by Typhoon in the South China Sea. *Bull. Sci. Technol.* **2018**, *34*, 57–63.
14. Doswell, C.A., III; Brooks, H.E.; Maddox, R.A. Flash Flood Forecasting: An Ingredients-Based Methodology. *Weather Forecast.* **1996**, *11*, 560–581. [CrossRef]
15. Liao, X.N.; Ni, Y.Q.; He, N.; Song, Q.Y. Analysis of the synoptic-scale dynamic process causing the extreme moisture environment in the "7.21" heavy rain case. *Acta Meteorol. Sin.* **2013**, *71*, 997–1011.
16. Lau, K.-M.; Zhou, Y.P.; Wu, H.-T. Have tropical cyclones been feeding more extreme rainfall? *J. Geophys. Res.* **2008**, *113*, D23113. [CrossRef]
17. Tao, S.Y. *Heavy Rainfalls in China*; Science Press: Beijing, China, 1980; pp. 1–225. (In Chinese)
18. Tao, S.Y.; Zhao, S.X.; Zhou, X.P.; Ji, L.R.; Sun, S.Q.; Gao, S.T.; Zhang, Q.Y. The research progress of the synoptic meteorology and synoptic forecast. *Chin. J. Atmos. Sci.* **2003**, *27*, 451–467.
19. Bian, Q.H.; Ding, Z.; Wu, M.Y. Statistical analysis of typhoon heavy rainfall in North China. *Meteorol. Mon.* **2005**, *31*, 61–65.
20. Sun, J.H.; Qi, L.L.; Zhao, S.X. A study on mesoscale convective systems of the severe heavy rainfall in North China by "9608" typhoon. *Acta Meteorol. Sin.* **2006**, *64*, 57–71.
21. Lei, L.; Sun, J.S.; He, N.; Liu, Z.; Zeng, J. A study on the mechanism for the vortex system evolution and development during the torrential rain event in North China on 20 July 2016. *Acta Meteorol. Sin.* **2017**, *75*, 685–699.
22. Zhao, S.X.; Sun, J.H.; Lu, R.; Fu, S. Analysis of the 20 July 2016 unusual heavy rainfall in North China and Beijing. *Meteorol. Mon.* **2018**, *44*, 351–360.
23. Zhang, D.L.; Lin, Y.H.; Zhao, P.; Yu, X.; Wang, S.; Kang, H.; Ding, Y. The Beijing Extreme Rainfall of 21 July 2012: "Right Results" but for Wrong Reasons. *Geophys. Res. Lett.* **2013**, *40*, 1426–1431. [CrossRef]
24. Luo, Y.L.; Gong, Y.; Zhang, D.L. Initiation and organizational modes of an extreme-rain-producing mesoscale convective system along a Mei-Yu front in East China. *Mon. Weather Rev.* **2014**, *142*, 203–221. [CrossRef]
25. Luo, Y.L.; Wu, M.W.; Ren, F.M.; Li, J.; Wong, W.K. Synoptic situations of extreme hourly precipitation over China. *J. Clim.* **2016**, *29*, 8703–8719. [CrossRef]
26. Pu, Y.; Hu, S.; Luo, Y.; Liu, X.; Hu, L.; Ye, L.; Li, H.; Xia, F.; Gao, L. Multiscale Perspectives on an Extreme Warm-Sector Rainfall Event over Coastal South China. *Remote Sens.* **2022**, *14*, 3110. [CrossRef]
27. Maddox, R.A. Mesoscale convective complexes. *Bull. Amer. Meteor. Soc.* **1980**, *61*, 1374–1387. [CrossRef]
28. Parker, M.D.; Johnson, R.H. Organizational modes of midlatitude mesoscale convective systems. *Mon. Weather Rev.* **2000**, *128*, 3413–3436. [CrossRef]
29. Huang, S. *Heavy Rain in South China during Pre-Flood Season*; Guangdong Science and Technology Press: Guangzhou, China, 1986; pp. 94–95.
30. He, L.F.; Chen, T.; Kong, Q. A review of studies on prefrontal torrential rain in South China. *J. Appl. Meteorol. Sci.* **2016**, *27*, 559–569.

31. Duan, B.L.; Zhang, W.L.; Liu, H.W.; Wang, X.Y. The spatial and temporal distributions of warm sector rainfall and frontal rainfall for the torrential rain event in Beijing on 21 July 2012. *Torr. Rain Dis.* **2017**, *36*, 108–117.
32. Chen, H.; Wang, Y.C.; Wei, Y.H.; Zhang, N.; Lin, X.M.; Yang, Y.; Zhang, Y.Q. Analysis of the Triggering and Maintenance Mechanisms of a Record-Breaking Warm-Sector Extreme-Rainfall Process in Front of an Upper-Level Trough in Tianjin, China. *Atmosphere* **2023**, *14*, 808. [CrossRef]
33. Zhou, M.F.; Du, X.L.; Xiong, W. Comparison Analysis of Two Warm Area Torrential Rain Systems in Early Summer in Guizhou. *Meteorol. Mon.* **2014**, *40*, 186–195.
34. Xiao, H.R.; Wang, J.J.; Xiao, D.X.; Long, K.J.; Chen, Y. Analysis of Warm-Sector Rainstorm Characteristics over Sichuan Basin. *Meteorol. Mon.* **2021**, *47*, 303–316.
35. Fu, Z.; Yang, X.J.; Zhou, X.J.; Liu, W.C. Analysis on Doppler Radar Characteristics of Warm Area Rainstorm in Southeastern Gansu during 19–20 June 2013. *Meteor. Mon.* **2015**, *41*, 1095–1103.
36. Xu, Y.; Zhang, G.H.; Meng, Y.Y.; Zhang, L.B. Analysis on the Formation of a Warm Sector Torrential Rain with Tornado in Heilongjiang Province. *Desert Oasis Meteorol.* **2020**, *14*, 40–48.
37. Chen, Y.; Chen, Y.; Chen, T.; He, H. Characteristics Analysis of Warm Sector Rainstorms over the Middle Lower Reaches of the Yangtze River. *Meteorol. Mon.* **2016**, *42*, 724–731.
38. Wang, L.Y.; Chen, Y.; Xiao, T.G.; Li, S.Q.; Ge, L. Statistical Analysis of Warm-Sector Rainstorm Characteristics over the Southern of Middle and Lower Reaches of the Yangtze River in Summer. *Meteorol. Mon.* **2018**, *44*, 771–780.
39. Shuai, H.; Shi, C.X.; Lin, H.J.; Meng, X.Y.; Lu, H.Q. The CLDAS soil moisture operation products applied to monitor soil drought. *J. Glaciol. Geocryol.* **2015**, *37*, 446–453.
40. Xiao, A.; Xu, A.H. Three hours negative pressure anomaly index and its significance in severe convective weather forecast. *Acta Meteorol. Sin.* **2018**, *76*, 78–91. [CrossRef]
41. Chen, B.F.; Ma, Z.Y.; Wang, L.Z.; Huang, L.; Li, Y.; Sheng, M.; Zhang, X. Echo Characteristics of Short-Term Heavy Rainfall Due to Severe Rainstorm in Changjiang River Basin, Jiangxi Province. *Meteorol. Mon.* **2022**, *48*, 1418–1427.
42. Hersbach, H.; Bell, B.; Berrisford, P.; Hirahara, S.; Horányi, A.; Muñoz-Sabater, J.; Thépaut, J.N. The ERA5 global reanalysis. *Q. J. R. Meteorol. Soc.* **2020**, *146*, 1999–2049. [CrossRef]
43. Tokay, A.; Petersen, W.A.; Gatlin, P.; Wingo, M. Comparison of raindrop size distribution measurements by collocated disdrometers. *Atmos. Ocean. Technol.* **2013**, *30*, 1672–1690. [CrossRef]
44. Zhang, G.F.; Vivekanandan, J.; Brandes, E.A.; Meneghini, R.; Kozu, T. The Shape–Slope Relation in Observed Gamma Raindrop Size Distributions: Statistical Error or Useful Information? *J. Atmos. Ocean. Technol.* **2003**, *20*, 1106–1119. [CrossRef]
45. Schumacher, R.S.; Johnson, R.H. Organization and environmental properties of extreme-rain-producing mesoscale convective systems. *Mon. Weather Rev.* **2004**, *133*, 961–976. [CrossRef]
46. Sun, J.S.; He, N.; Guo, R.; Chen, M.X. The Configuration Change and Train Effect Mechanism of Multi-Cell Storms. *Chin. J. Atmos. Sci.* **2013**, *37*, 137–148. (In Chinese) [CrossRef]
47. Bao, H.M.; Xiao, A.; Li, W.; Qian X., C. Characteristics of Specific Humidity in South China and Its Relationship with Rainstorm. *Meteorol. Env. Sci.* **2021**, *44*, 33–42.